VNU Journal of Science: Mathematics - Physics
Journal homepage: https://js.vnu.edu.vn/MaP

Original Article

Structural Properties of Amorphous Vanadium Pentoxide Under Compression

Nguyen Thu Nhan*

Hanoi University of Science and Technology, 1 Dai Co Viet, Hanoi, Vietnam

Received 23 August 2023
Revised 06 November 2023; Accepted 22 April 2024

Abstract: Structural properties of amorphous vanadium pentoxide (V_2O_5) under compression have been investigated by molecular dynamics simulation. A simulated amorphous V_2O_5 was composed of basic structural units of type VO_5, VO_6 at low-pressures and VO_6, VO_7 at high-pressures. These basic structural units were connected by vertex-, edge- and face- shared links to form a structural network. The random distribution of atoms and void clusters led to a high degree of disorder in V_2O_5 structure. Under compression, the fraction of average vertex-, edge- and face- shared links increased strongly. The number of void clusters (VCs) and void tubes (VTs) also increased as the large voids are divided into smaller voids. The obtained results demonstrate that the decreasing of cross-section and increasing of length in VTs mainly cause increasing the ion conductivity of amorphous V_2O_5.

Keyworks: Amorphous V_2O_5, void, link, compression, molecular dynamics.

1. Introduction

Among materials used as electrodes for fuel cells like V_2O_5, CoO_2, TiO_2, MnO, $FePO_4$, etc., V_2O_5 has received the most research attention in recent years [1-10]. V_2O_5 used as electrode materials have advantages such as high energy density and capacitance, good cyclic stability, and fast electron transfer. When pressure and/or temperature changes, V_2O_5 undergoes a structural phase transition leading to a variety of energy storage capacity as well as the diffusion rate of charged ions. When a b-V_2O_5 sample is compressed at 6.0 GPa and annealed at 1,073 K, V atoms possess 6-coordination by oxygens and VO_6 octahedra are distorted [11], forming clusters. Each cluster consists of four VO_6 units that have an edge- and /or a vertex-sharing link. Crystalline V_2O_5 consist of V_4O_{10} layers which are weakly linked together. The bond lengths of V-V, V-O, and O-O in a structural unit also vary and depend on the link types of

* Corresponding author.
E-mail address: nhan.nguyenthu@hust.edu.vn

https//doi.org/10.25073/2588-1124/vnumap.4869

edge- or vertex-sharing. At 643 – 653 K, there is a phase transition from b-V_2O_5 to α-V_2O_5 structure. Baddour-Hadjean et al., [12] showed that the structural phase transition from α- to b-V_2O_5 occurred under compressing at 8.0 GPa and annealing at 1,073 K. The obtained results in [13, 14] showed a shift of coordination numbers from 5- coordinated to 6- coordinated of V atoms at 7.0 GPa. With increasing pressure, the V-O bond distance within a layer increased slightly, while the V-O distance between layers decreased strongly. X-ray diffraction patterns carried out at temperatures from 12 K to 853 K did not show any evidence of structural phase transition or decomposition of α-V_2O_5 [15]. Amorphous V_2O_5 annealed at 400 °C undergoes a structural phase transition from amorphous to layered polycrystalline structures [16]. Between layers of the polycrystalline V_2O_5, Li+ ions easily inserted, resulting in the increase of the charge capacity of the samples. Dompablo et al., [17] showed that at room temperature, the resistivity of V_2O_5 at high pressures is smaller than the one at low pressures. This proves that crystalline V_2O_5 compressed at high pressures has better ability to transport and to store energy. This is due to the reduced band gap leading to the increase of the conductivity of the V_2O_5. Recently, amorphous V_2O_5 has attracted more attention as an electrode in comparison with crystalline V_2O_5 due to the disorder of the amorphous structure. Structural disorder created natural conduction channels for charge-carrying atoms strongly diffusive in it, thereby increasing the electrical conductivity of the materials [10, 18-21]. This hypothesized that the amorphous structure provides more space than the crystal in ion storage and transport. Vu et al., [18] also confirmed that the charge, discharge, and energy storage capacity of amorphous V_2O_5 is better than that of crystalline V_2O_5. However, the correlation between the structural order and the semiconductor properties of amorphous V_2O_5 is still an open question to be elucidated. The role of the free volume region, which provides space for the movement and storage of ions in the amorphous V_2O_5 structure, has never been studied. The ability to store energy of V_2O_5 materials is much dependent on their microstructural properties such as chemical bonds, size of atom clusters and the size and shape of free volumes.

To elucidate these issues, a detailed study of the microstructure of amorphous V_2O_5 under pressures is neccessary. The spatial distributions of atoms, the link distributions and the geometrical distributions of the free volumes need to be fully investigated. The distribution of free volumes in the amorphous V_2O_5 network also needs to be visualized. Thisis just the main contents of our work.

2. Calculation Method

A model V_2O_5 consisting of 3,003 atoms (858 V atoms and 2,145 O atoms) is built by molecular dynamics (MD) at 300 K and pressures in the range 0-40 GPa, under periodic boundary conditions. The Born-Meyer interaction potential used in model building has the form:

$$U_{ij}(r) = q_i q_j \frac{e^2}{r_{ij}} + B_{ij}\, exp(-\frac{r_{ij}}{R_{ij}})$$

where the ionic charges of V and O are q_V=5, q_O=-2, respectively. The pair interaction coefficients $B_{V\text{-}V}$=0, $B_{V\text{-}O}$=2970, $B_{O\text{-}O}$=1500 eV and R_{ij}=29 pm. We use these interaction potentials because they allow reconstruction of the amorphous V_2O_5 structure giving results that are in good agreement with the experimental data [8, 22]. First, we randomly put 3,003 points in a cube with density 3.35 g/cm^3 (experimental density of V_2O_5 at boundary pressure and room temperature). The system relaxed for 10^3 MD steps to remove the initial state. Next, the system is heated to 6,000 K for about 5.10^4 MD steps to ensure that the physics of the interaction potential at zero distances are not disrupted. Then, this high-temperature model cooled rapidly down to 300 K at 0.25 K ps^{-1}. At this temperature, the model relaxed over 5.10^3 MD steps. The system continued to run until a stable equilibrium (approximately 10^8 MD

steps) at 0 GPa. The different pressure models generated as follows: first, the model at 0 GPa compressed to 5, 10, 15, 20, 25, 30 and 40 GPa over 10^6 MD steps and kept the parameters N (moles), P (pressure) and T (temperature) constant. Next, these compression models run until equilibrium after 10^8 MD steps. The radial distribution function is averaged calculation after 10^4 configurations and compared with experiment. Other structural features such as coordination numbers, bond length and bond angle distribution are also calculated. The uniform distribution of atoms into a cluster, the statistics of the links sharing vertices, edges and faces among the basic structural units are investigated in detail.

To provide information about the ability to insert impurity atoms into the built model, we carry out statistical calculations of the distribution of voids in the free space of the model. The covalent radii of V and O atoms are of 1.22 Å and 0.73 Å respectively. Detailed calculations of the void distribution can be found in [23]. A void cluster (VC) defined as the largest void in the center that is partially overlapped by the surrounding smaller voids. A void tube (VT) defined as voids that overlap to form a series. These VCs and VTs have a cross-sectional radius greater than or equal to the radius O and they are holes or paths where O atoms can diffuse. From the distribution of CVs and VTs, one can explain the increase in the ability to store and transport charged ions under compression. We show an optimum pressure value at which the system can store as well as transmit charged ions.

3. Results and Discussions

3.1. Structural Characteristics

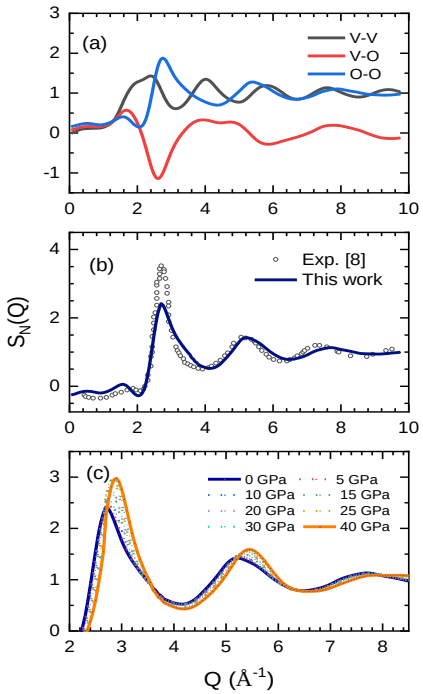

Figure 1. The neutron scattering structure factor, $S_N(Q)$, of amorphous V_2O_5 at 300 K under compression.

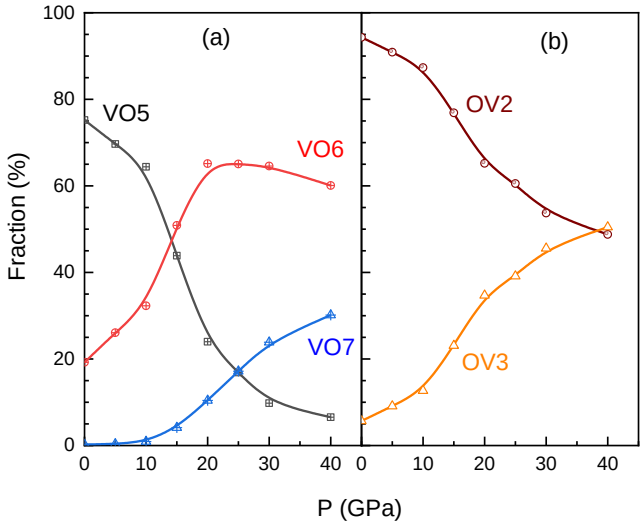

Figure 2. Distribution of VO_x (x=5,6,7) and OV_y (y=2,3) coordination units under compression.

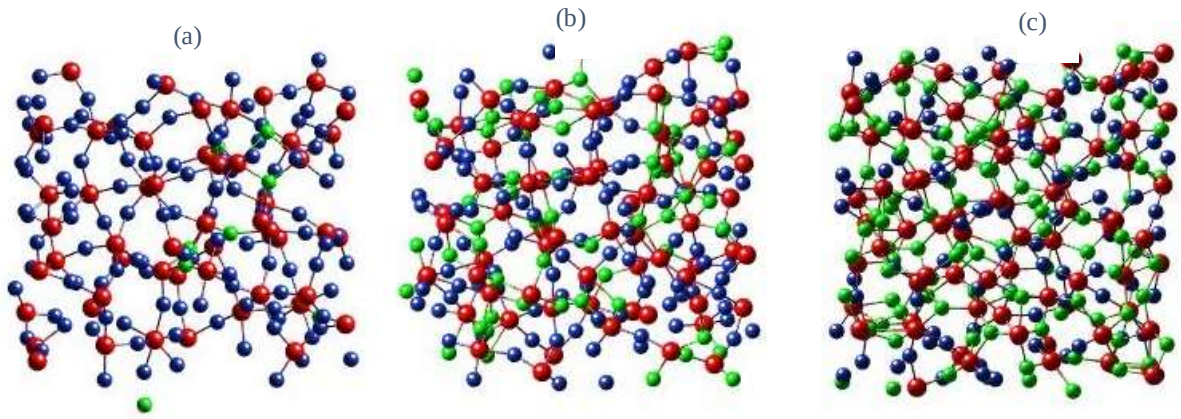

Figure 3. A visualization of the O atoms with DVL (blue O) and TVL (green O) at pressures of (a) 0 GPa, (b) 20 GPa and (c) 40 GPa in size 12x5x12 (Å). Note that the red sphere is the V atom.

The pair netron scattering structure factor of V_2O_5 at 300 K and 0 GPa has been calculated by using a set of coordinate positions (Fig. 1a). The total neutron scattering structure factor (Fig. 1b) is determined and compared with the experimental data in [8]. At pressure of 0 GPa, three main peaks of Q are 2.7, 5.2 and 7.6 $Å^{-1}$. When increasing compression, the position of peaks shifts to a larger Q (Fig. 1c). At 40 GPa, the positions of the peaks are of 2.9, 5.45 and 7.8 $Å^{-1}$. It proves that there is a change in the structural network with compression. This change is elucidated by the fraction of the basic structural units VO_x (x is the number of O atoms) and OV_y (y is the number of V atoms) (see Fig. 2). At 0 GPa, the structure mainly comprises the mixture of VO_5 and VO_6 units, about 75% and 20%, respectively. The number of VO_7 units is very small, about 0.2%. As the compression increases, the fraction of VO_6 units increases and reaches its maximum value at 20-25 GPa and then decreases slightly in the range of 30-40 GPa. The VO_5 fraction decreased rapidly from 75% to approximately 6% and fraction of VO_7 units continuously increased from 0.2 to 30% with increasing pressure from 0-40 GPa (see Fig. 2a). Thus, at high pressures, the V_2O_5 structure mainly comprises the mixture of VO_6 and VO_7 units. These

basic structural units are linked together by O-shared atoms to form a second structural unit type OV_y. The fraction of OV_y under compression calculated (Fig. 2b). At low pressures, most O atoms are linked to 2 V atoms with a fraction of 94%. An O linked with two neighboring V atoms called a double-vertex link (DVL). Its fraction decreases from 94% to 50% when compression increases from 0-40 GPa. We also observed that only about 6% O linked to 3 V atoms and called a three-vertex link (TVL). Fraction of OV_3 increases from 6% to 50% as the pressure increases from 0-40 GPa. At 40 GPa, the DVL and TVL fractions are equal, that is, the structural network consists of structural units VO_6, VO_7 and they connect by O atom with DVL and/or TVL. At 20-25 GPa, the number of VO_6 units is the largest. Links between VO_6-VO_6, VO_6-VO_5, VO_5-VO_5 found in DVLs and a few TVLs. Figure 3 shows the distribution of oxygens with DVLs and TVLs at 0, 20 and 40 GPa.

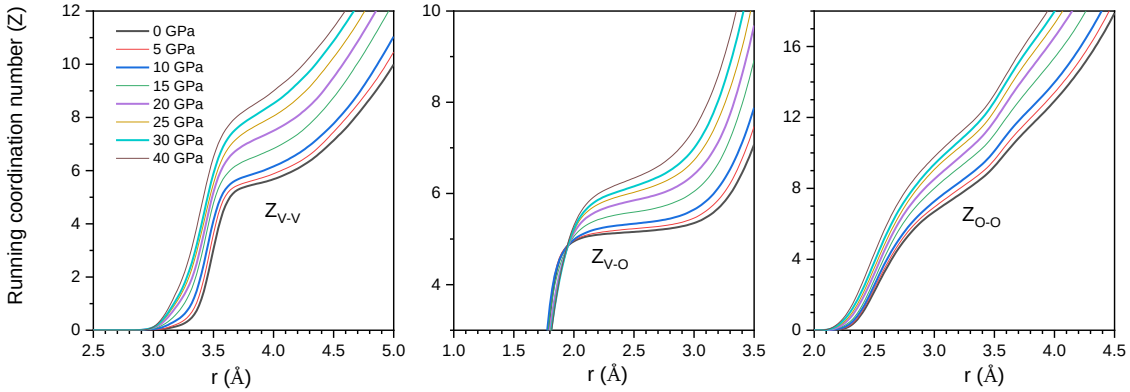

Figure 4. Running coordination number of V and O atoms under compression.

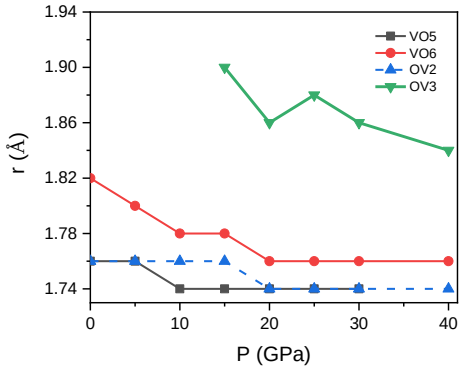

Figure 5. Maximum peak position of bond distance distribution O-V in units VO_5, VO_6, OV_2 and OV_3 under compression.

The local environment of V and O atoms become denser under compression. The coordination number of atoms increases due to the bond distance decreasing to form links. Fig. 4 shows that the coordination number of atoms dependent on r (with r is the radius of the coordination sphere). The running coordination number is defined by the change in the number of coordination atoms in a coordination sphere as r changes. It is seen that the coordination number increases both as r and/or pressure increases. The strongest change is the O-O pair coordination number; it changes from 6-coordinated to 11-coordinated as the distance increases from 2.6-3.7 Å. The V-V pair coordination

numbers also change from 5- to 7-coordinated in the range of 3.5-4.4 Å. With V-O pairs, the coordination number varies from 5- to 7-coordinated between 1.75-3.50 Å. As the compression increases, the curve slope of V-V and O-O pair coordination numbers increase. We see that only an insignificant change in distance also leads to an increase in the number of links between atoms, thereby increasing coordination coordinates. For the V-O pair, the bond distance change is analyzed in Fig. 5. It displays the position of the peaks of the V-O distance distribution function in short-order (the V-O distance in a basic structural unit) and the O-V distance in the mid-range order (the O-V distance between two neighboring structural units). The V-O distance in VO_5 decreases from 1.76 Å to 1.74 Å as the pressure increases from 5-10 GPa. The V-O distance in VO_6 decreases gradually in the pressure range from 0-20 GPa.

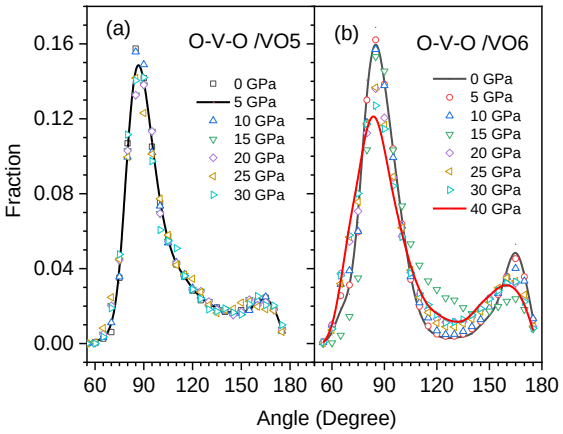

Figure 6. Bond angle distribution O-V-O in (a) VO_5 and (b) VO_6 units under compression.

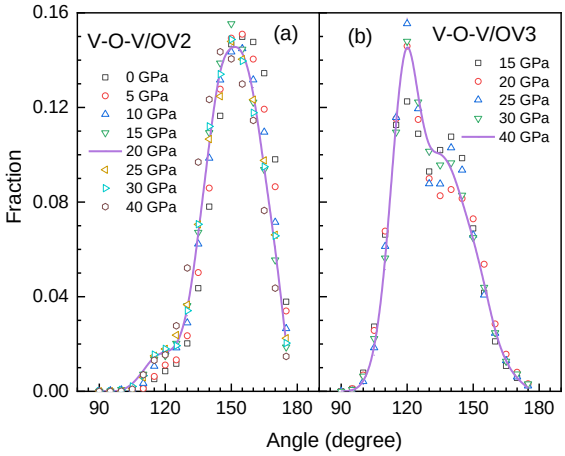

Figure 7. Bond angle distribution V-O-V in (a) OV_2 and (b) OV_3 units under compression.

The above analysis has shown that, at low pressures, the structural network exists in two regions: weak and strong bonds. Strongly bound regions are regions formed by clusters of VO_5 structural units with DVLs and TVLs (Fig. 6a and Fig. 7b). As the pressure increases, only the O-V distance in the TVLs decreases, the averaged bond angle of VO_5 and OV_3 are unchanged. The weakly bound region is the region made up of VO_6 units linked together via DVLs and TVLs. Under compression, the geometric structure of VO_6 changes both bond distance and angle. At high pressure (above 20 GPa) the geometry structure of VO_6 becomes stable with main DVLs (Fig. 5). The structure becomes denser with the appearance of face bonds due to reducing V-O bond distance in the TVLs. The cluster distribution of the basic structural units shown in Table 1. At pressures below 15 GPa, the structural network is VO_5 units linked together to form a large cluster spread throughout the model. The number of atoms in the largest VO_5 cluster decreases under compression. A decrease in V-O bond distance leads to an increase in link number that forms the 6-coordinated number. The small VO_6 clusters are more extensive while the VO_5 clusters tend to shrink, links broken to form discrete clusters. At a pressure of 15 GPa, the system has two main VO_5 and VO_6 clusters. In addition, there are small clusters of VO_5, VO_6 and VO_7. At high pressures above 20 GPa, the large VO_6 cluster expands into the largest cluster containing 2469 atoms, accounting for 82% of the total number of atoms in the model. This cluster expanded under compression. It can be seen in Fig. 8, the V-O bond distance decreases, leading to an increase in the number of vertex-, edge- and face-shared. At a pressure of 0 GPa, atom V is bonded by 5 O atoms, in which there are 2.67 vertex-shared, 0.09 edge-shared and 0.0035 face-shared links.

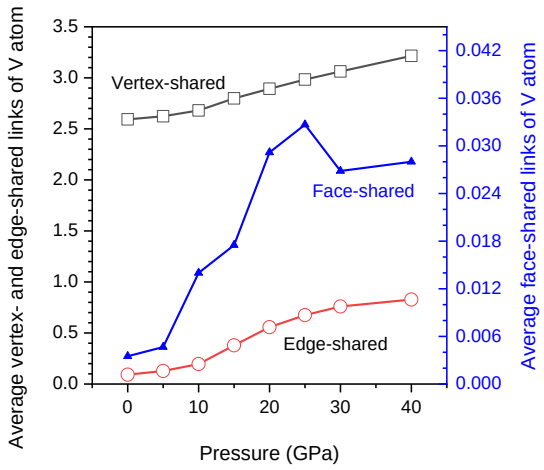

Figure 8. The number of average vertex-, edge- and face-shared links of V atom.

Table 1. Cluster distribution of structural units VO_5, VO_6, and VO_7 under compression. N_c and N_a are the number of clusters and number of atoms in per cluster, respectively

	0 GPa		**5 GPa**		**10 GPa**		**15 GPa**	
	N_c	N_a	N_c	N_c	N_a	N_a	N_a	N_a
VO_5	1	**2632**	1	**2597**	1	6	25	6-28
					1	**2425**	1	**1714**
VO_6	69	7-93	65	7-95	32	7-55	4	7-19
	1	133	1	144	1	370	1	**2060**
					1	799		
VO_7	2	8	2	8	6	8-14	24	8-22
	20 GPa		**25 GPa**		**30 GPa**		**40 GPa**	
	Nc	Na	Nc	Na	Nc	Na	Nc	Na
VO_5	52	6-94	60	6-58	65	6-56	44	6-23
	3	121-234	1	253				
VO_6	1	7	1	**2495**	1	**2576**	1	**2479**
	1	**2469**						
VO_7	42	8-27	52	8-85	43	8-95	18	8-52
					1	231	1	258
							1	974

The vertex- and edge-sharings increase rapidly with compression. For example, at 30 GPa, each V atom has 3.0 vertex-shared and 0.75 edge-shared links. The fraction of links increases rapidly in the range of 10-25 GPa and is shown in the steepest part of the graph in Fig. 8. The fraction of face-shared links is quite small. Fig. 9 is a visualization of vertex-, edge-, and face-shared links at 0, 25 and 40 GPa. At 0 GPa, the structural units are connected by vertex-shared links. Only a few links are edge-shared (Fig. 9a). The number of vertex- and edge-shared links increases rapidly when increasing compression and the number of face-shared links increases to the maximum value at 25 GPa (see Fig. 8 and Fig. 9b). We predict that, under compressions up to over 20 GPa, the large CVs are shrunk by increasing in vertex-, edge-, and face-linking. At above 25 GPa, the number of vertex- and edge-shared links keep growing, but the face-shared links decrease significantly (Fig. 9c).

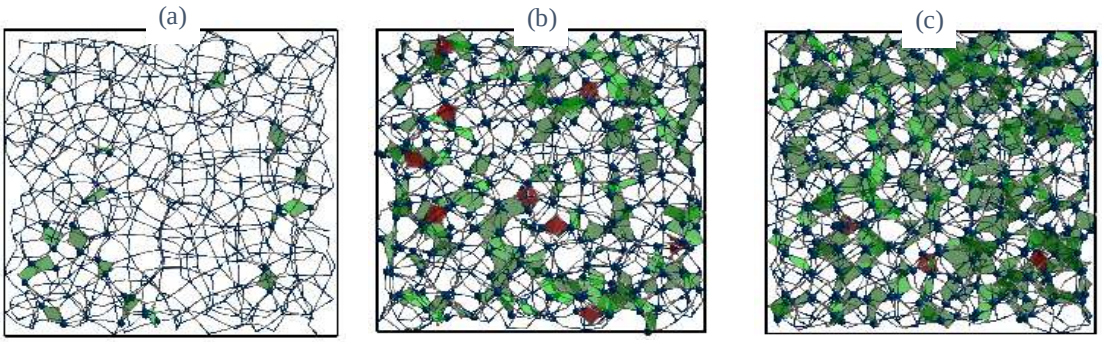

Figure 9. A visualization of vertex-, edge-, and face-shared links in size 12x5x12 (Å) at: (a) 0 GPa, (b) 25 GPa and (c) 40 GPa. Where the solid line is vertex-shared link, green plane is edge-shared link and red polyhedron is face-shared link.

3.2. Free Volume Distribution and Visualization

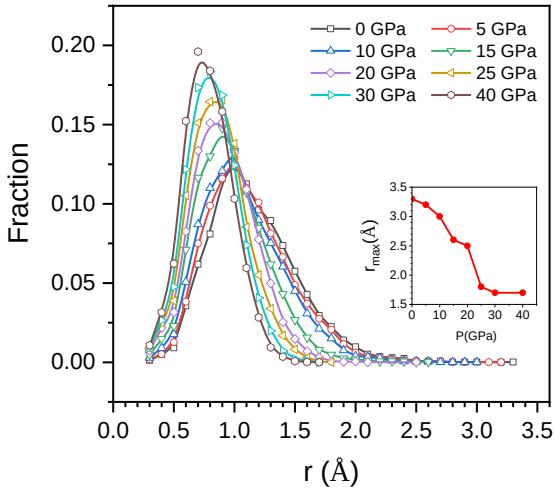

Figure 10. The distribution of void radius (r, outside graph) and maximum void radius (r_{max}, inside graph) under compression.

The amorphous material V_2O_5 provides large free volume regions where no atom can occupy. The distribution of free volumes plays a key role in assessing the ability to store and move charged ions in the structural network. Furthermore, the diffusion of charged ions depends not only on the chemical property of the molecules (i.e., on the bond between atoms) but also on the local natural environment. By placing the spheres in contact with four neighboring atoms we have given the radius distribution of the set of voids as seen in Fig. 10. It shows the peak shift in the radius distribution function from 1 Å to 0.7 Å under compression. The largest void radius, r_{max}, decreases rapidly from 3.3 Å to 1.7 Å when the pressure increases from 0-40 GPa (see small figure inserted inside Fig. 10). Especially, at 20-25 GPa, the number of largest voids decreases quickly. It shows that the density of the model increases due to the free volume decreasing. Voids are greater than or equal to the oxygen atom considered as vacancies

and it is significant in the diffusion mechanism of the system. Table 2 shows the distribution of vacancies under compression.

Table 2. Free volume characteristics in amorphous V_2O_5 systemunder compression. N_V, N_{VC}, N_{VT} and N_{LVT} are the number of voids, clusters, tubes and of voids in the largest tube, respectively. V_T and V_V are the fraction of tube and void volume with model volume, respectively

P (GPa)	0	5	10	15	20	25		30	40
N_V	12185	12683	13238	14510	15116	15116		16369	16824
N_{VC}	2199	2437	2772	2622	2874	3907		4208	4562
N_{VT}	184	221	265	391	484	604		-	-
N_{LVT}	11099	11336	11468	11809	11307	10490		-	-
V_T	0.63	0.62	0.6	0.55	0.49	0.42		-	-
V_V	0.6544	0.6454	0.633	0.6029	0.5731	0.5512		0.5341	0.5142

The number of vacancies increased from 12,185 at 0 GPa to 16,824 at 40 GPa. The number of void clusters, N_{VC}, also increased linearly with the compression from 2,199 clusters at 0 GPa to 4,562 clusters at 40 GPa. The number of void tubes, N_{VT}, only found below 30 GPa. When the compression increases, N_{VT} increases, the number of vacancies in a VT also increases, but average cross-section (d_a=average diameter of a VT) decreases. The d_a of VTs at 5, 10 and 20 GPa are 4.5, 4.0 and 3.6 Å, respectively. This can be explained as follows, under compression, the decrease in bond length leads to an increase in the number of links, thus dividing the large free volume into small vacancies. It also caused increases in N_{VC} and N_{VT}. VTs distributed randomly in a structural network and VCs also sometimes belong to the largest VT.

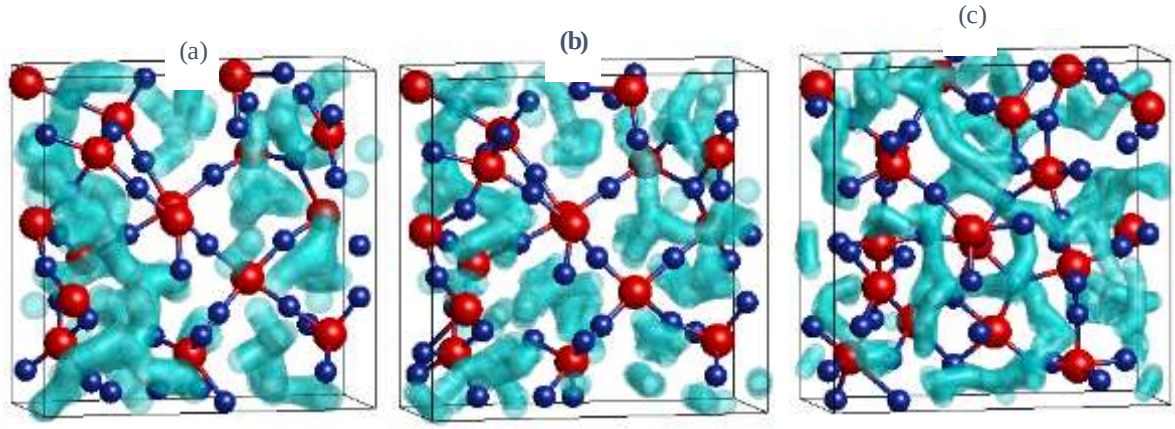

Figure 11. A snapshot of distribution of atoms V(red), O (blue), and parts of the largest VT (light blue) in size 12x5x12 (Å) at (a) 5 GPa, (b) 10 GPa and (c) 20 GPa.

The distribution of VC and VT visualized in Fig. 11 at 5, 10 and 20 GPa with size 12×5×12 Å. This is a snapshot of the model with a thickness of 5 Å, so it only reflects part of the structure and some segments of the largest VT. Similarly, the polycrystalline, V_2O_5 has a layered structure, when compacting the distance between the layers narrowed leading to better ionic conductivity [17]. The model of amorphous V_2O_5 when compressed, there is a decreasing in cross-section and increasing in length of the VTs with branches lying in the amorphous structure network. They are the void trees that

permeate through the V_2O_5 structural network. With charge-balanced properties, distribution of VTs will attract positive ions moving in the structural network and increase the ionic conductivity of amorphous V_2O_5. At pressures larger 30 GPa, VTs were not observed. In this simulation, we have shown that at pressures 20 - 25 GPa, the number of VTs is maximum and their cross-section reduced to an appropriate value, thereby increasing the conductivity of amorphous V_2O_5.

4. Conclusions

The report has given a general picture of the amorphous V_2O_5 and the distribution of VCs and VTs in the structural network under compression. At 0 - 15 GPa, the structure of the system mainly comprises VO_5 and VO_6 units linked together by DVL. At high pressures (f.i. 40 GPa), the V_2O_5 structure is mainly formed by VO_6 and VO_7 units linked together through the vertex-shared (including DVL and TVL) and edge-share links. There are a few face-shared links. At 20 - 25 GPa, the structural network consists of VO_6, VO_5 and VO_7 clusters in which the VO_5 and VO_7 small clusters are distributed randomly in the largest cluster VO_6. The number of TVL links has quickly increased. The increasing number of vertex-, edge-, and face-shared links under compression causes the cluster of basic structural units to expand, the free volume region to shrink. This free volume distributes under cluster or tube shape and depends on the compression pressure. The obtained results have clarified two issues: i) The electrical conductor of amorphous V_2O_5 is better than of crystalline V_2O_5; and ii) The conductivity of amorphous V_2O_5 at high pressures is better than at low pressures? In the amorphous structure, there are large voids with radii ranging from 0.73 to 3.3 Å. These voids may be single or overlap to form large clusters or long tubes. Under compression up to 25 GPa, these large clusters and long tubes shrunk and interconnected. Thus, the tubes become longer but cross-sectional is narrower when comparing with 0 GPa. These results originate from increasing conductivity of amorphous V_2O_5 under compression.

References

[1] C. Sanchez, J. Livage, G. Lucazeau, Infrared and Raman Study of Amorphous V2O5, Journal of Raman Spectroscopy, Vol. 12, No. 1, 1982, pp. 68-72, https://doi.org/10.1002/jrs.1250120110.

[2] S. Wu, Y. Ding, L. Hu, X. Zhang, Y. Huang, S. Chen, Amorphous V_2O_5 as High-performance Cathode for Aqueous Zinc Ion Battery, Mater. Let., Vol. 277, 2020, pp. 128268, https://doi.org/10.1016/j.matlet.2020.128268.

[3] A. Kuddus, M. F. Rahman, S. Ahmmed, J. Hossain, A. B. M. Ismail, Role of Facile Synthesized V_2O_5 as Pore Transport Layer for CdS/CdTe Heterojunction Solar Cell: Validation of Simulation Using Experimental Data, Super, and Micro., Vol. 132, 2019, pp. 106168, https://doi.org/10.1016/j.spmi.2019.106168.

[4] S. Petnikota, R. Chua, Y. Zhou, E. Edison and M. Srinivasan, Amorphous Vanadium Oxide Thin Films as Stable Performing Cathodes of Lithium and Sodium-Ion Batteries, Nano. Res. Let. Vol.13, 2018, pp. 363, https://doi.org/10.1186/s11671-018-2766-0.

[5] A. Gaddam, A. R. Allu, H. R. Fernandes, G. E. Stan, C. C. Negrila, A. P. Jamale, J. M. F. Ferreira, Role of Vanadium Oxide on The Lithium Silicate Glass Structure and Properties, J. Ame. Ceram. Soc., Vol. 104, 2021, pp. 2495-2505, https://doi.org/10.1111/jace.17671.

[6] H. O. Tekin, S. A. M. Issa, G. Kilic, H. M. H. Zakaly, M. M. Abuzaid, N. Tarhan, M. H. M. Zaid, In-Silico Monte Carlo Simulation Trials for Investigation of V2O5 Reinforcement Effect on Ternary Zinc Borate Glasses: Nuclear Radiation Shielding Dynamics, Mater, Vol. 14, 2021, pp. 1158, https://doi.org/10.3390/ma14051158.

[7] J. Lee, A. Urban, X. Li, D. Su, G. Hautier, G. Ceder, Unlocking the Potential of Cation-Disordered Oxides for Rechargeable Lithium Batteries, Sci. Vol. 343, 2014, pp. 519, https://doi.org/10.1126/science.1246432.

[8] H. Munemura, S. Tanaka, K. Maruyama, M. Misawa, Structural Study of Li_2O–V_2O_5 Glasses by Neutron and X-ray Diffraction, J. Non-Cryst. Solids, Vol. 312-314, 2002, pp. 557, https://doi.org/10.1016/s0022-3093(02)01770-2.

[9] W. Li, S. H. Garofalini, Molecular Dynamics Simulations of Li Insertion in a Nanocrystalline V2O5 Thin Film Cathode, J. Elec. Soc., Vol. 152, 2005, pp. A364, https://doi.org/10.1149/1.1848345.

[10] E. Uchaker, Y. Zheng, S. Li, S. L. Candelaria, S. Hu, G. Cao, Better than Crystalline: Amorphous Vanadium Oxide for Sodium-ion Battery, J. Mater. Chem. A, Vol. 2, 2014, pp. 18208-18214, https://doi.org/10.1039/C4TA03788J.

[11] V. P. Filonenko, M. Sundberg, P. E. Werner, I. P. Zibrov, Structure of a High-pressure Phase of Vanadium Pentoxide, Acta Cryst. B, Vol. 60, 2004, pp. 375-381, https://doi.org/10.1107/s0108768104012881.

[12] R. B. Hadjean, M. B. Smirnov, K. S. Smirnov, V. Y. Kazimirov, J. M. G. Amores, U. Amador, J. P. P. Ramos, Lattice Dynamics of β-V_2O_5: Raman Spectroscopic Insight into the Atomistic Structure of a High-Pressure Vanadium Pentoxide Polymorph, Inorg. Chem., Vol. 51. 2012, pp. 3194-3201, https://doi.org/10.1021/ic202651b.

[13] I. Loa, A. Grzechnik, U. Schwarz, K. Syassen, M. Hanfland, R. K. Kremer, Vanadium Oxides V_2O_5 and NaV_2O_5 under High Pressures: Structural, Vibrational, and Electronic Properties, J. Alloy. Comp. Vol. 317-318, 2001, pp. 103-108, https://doi.org/10.1016/s0925-8388(00)01404-3.

[14] A. Grzechnik, Local Structures in High Pressure Phases of V_2O_5, Chem. Mater., Vol. 10, 1998, pp. 2505-2509, https://doi.org/10.1021/cm980245z.

[15] B. Singh, M. K. GuHTa, S. K. Mishra, R. Mittal, P. U. Sastry, S. Rols, S. L. Chaplot, Phys. Anomalous Lattice Behavior of Vanadium Pentoxide (V_2O_5): X-ray Diffraction, Inelastic Neutron Scattering and AB Initio Lattice Dynamics, Chem. Chem. Phys., Vol. 19, 2017, pp. 17967-17984, https://doi.org/10.1039/c7cp01904a.

[16] T. C. Lin, B. J. Jheng, H. M. Yen, W. C. Huang, Thin Film as an Ionic Storage Layer for Electrochromic Application, Mater., Vol. 15, 2022, pp. 4598, https://doi.org/10.3390/ma15134598.

[17] M. E. A. Dompablo, U. Amador, J. M. G. Amores, C. Baehtz, N. Biskup, E. Morán, High Pressure Materials for Energy Storage: The Case of V_2O_5, J. Phys.: Confer. Seri., Vol. 121, 2008, pp. 032001, https://doi.org/10.1088/1742-6596/121/3/032001.

[18] S. Wu, Y. Ding, L. Hu, X. Zhang, Y. Huang, S. Chen, Amorphous V_2O_5 as High-performance Cathode for Aqueous Zinc Ion Battery, Mater. Let., Vol. 277, 2020, pp. 128268, https://doi.org/10.1016/j.matlet.2020.128268.

[19] A. Mosset, P. Lecante, J. Galy, J. Livage, Structural Analysis of Amorphous V_2O_5 by Large-angle X-ray Scattering, Phi. Mag. B, Vol. 46, 1982, pp.137-149, https://doi.org/10.1080/13642818208246430.

[20] H. Xiong, M. D. Slater, M. Balasubramanian, C. S. Johnson, T. Rajh, Amorphous TiO_2 Nanotube Anode for Rechargeable Sodium Ion Batteries, J. Phys. Chem. Let., Vol. 2, 2011, pp. 2560-2565, https://doi.org/10.1021/jz2012066.

[21] H. T. Fang, M. Liu, D. W. Wang, T. Sun, D. S. Guan, F. Li, H. M. Cheng, Comparison of the Rate Capability of Nanostructured Amorphous and Anatase TiO_2 for Lithium Insertion Using Anodic TiO_2 Nanotube Arrays, Nanotech., Vol. 20, 2009, pp. 225701, https://doi.org/10.1088/0957-4484/20/22/225701.

[22] T. Aoyagi, S. Kohara, T. Naito, Y. Onodera, M. Kodama, T. Onodera, H. Takizawa, Controlling Oxygen Coordination and Valence of Network Forming Cations, Scien. Reports, Vol. 10, 2020, pp. 7178, https://doi.org/10.1038/s41598-020-63786-y.

[23] P. K. Hung, L. T. Vinh, D. M. Nghiep, P. N. Nguyen, Computer Simulation of Liquid Al_2O_3, J. Phys.: Condens. Matter, Vol. 18, 2006, pp. 9309-9322, https://doi.org/10.1088/0953-8984/18/41/001.